STRUCTURAL EVOLUTION IN LASER TREATED Ag/Co MULTILAYERS WITH GIANT MAGNETORESISTANCE

A. Anopchenko [1], M. Jergel [1], V. Holý [2], E. Majková [1], M. Spasova [1], Š. Luby [1], M. Brunel [3], A. Luches [4], M. Martino [4]

[1] *Institute of Physics of the Slovak Academy of Sciences, Dúbravská cesta 9, 842 28 Bratislava, Slovakia,*

[2] *Laboratory of Thin Films and Nanostructures, Masaryk University, Kotlářská 2, 611 37 Brno, Czech Republic*

[3] *Laboratoire de Cristallographie du CNRS, B.P.166, 38042 Grenoble Cedex 09, France*

[4] *I.N.F.M. and University of Lecce, Department of Physics, 73100 Lecce, Italy*

Abstract

An interplay between the structure and giant magnetoresistance (GMR) in laser treated Ag/Co multilayers (MLs) is studied. Three samples with different Ag layer thicknesses, denoted according to nominal values (in nm) as Ag_2Co_1, Ag_4Co_1, and Ag_6Co_1, were exposed to XeCl excimer laser pulses of the fluences (0.1-0.25) Jcm^{-2} for (1-200) times. The structure was examined by X-ray diffraction, X-ray reflectivity, and diffuse scattering measurements at grazing incidence. The polycrystalline face-centered cubic structure of Ag layers with random orientation of the grains was found in as-deposited Ag_2Co_1 and Ag_6Co_1. The formation of a discontinuous ML by grain boundary diffusion of Ag into Co layers induced by laser treatment is evidenced in Ag_6Co_1 which explains a systematic increase of the GMR before Ag layers start melting. The melting of Ag layers starts at too low laser fluence to complete such a process in Ag_2Co_1. A strong texture of Ag layers found in Ag_4Co_1 stabilizes the as-deposited structure and prevents from a systematical increase of the GMR. When Ag layers start melting, the ML structure is lost and rapid solidification results in a granular-like structure. This structure need not be optimal for achieving a high GMR value.

Keywords: multilayers, X-ray reflectivity, giant magnetoresistance, diffuse scattering, grazing incidence diffraction,

1. Introduction

The giant magnetoresistance (GMR) effect in magnetic/non-magnetic multilayers (MLs) was discovered in 1988 [1]. Magnetic moments in the magnetic layers separated by non-magnetic ones are coupled antiferromagnetically. The parallel alignment of magnetic moments achieved in an external magnetic field brings about a pronounced decrease of the electrical resistance. The theoretical explanation of this effect is based on the spin-dependent interface electron scattering [2].

A lot of effort has been devoted to an enhancement of the GMR effect in MLs by a post-deposition thermal treatment. A laser optimization of the GMR has been absent in the literature though it has more advantages. It enables us to deposit a required amount of energy into the volume of a thin film without heating the substrate. This amount is controlled by two independent parameters – fluence and number of pulses. Recently, we have started the studies of the effect of excimer laser irradiation on the GMR in Ag/Co MLs [3,4]. We have found that the GMR may be enhanced nearly twice provided the solid-state diffusion can take place up to high enough laser fluences before Ag layers start melting. The enhancement of the GMR was supposed to be due to the formation of a discontinuous ML. The formation of such discontinuous MLs with enhanced GMR was reported for some traditionally annealed MLs [5-7]. In this work, we concentrate on an interplay between the GMR results obtained previously and the underlying structural changes induced by excimer laser irradiation. A complex structural study of Ag/Co MLs is performed including X-ray diffraction (XRD), X-ray reflectivity (XRR) and grazing incidence diffuse scattering (GIDS) measurements.

2. Experimental

The sample preparation and laser treatment are described in more detail in Refs. [3,4]. Three samples nominally (2 nm Ag/1 nm Co)x5, (4 nm Ag/1 nm Co)x10, (6 nm Ag/1 nm Co)x5 were deposited by electron beam evaporation, starting with Ag, on Si(100) wafer covered with a 0.3 μm thick SiO_2 passivation layer. They are labelled further as Ag_2Co_1, Ag_4Co_1, Ag_6Co_1, respectively.

The thermal treatment was performed by excimer XeCl laser with laser fluences F = 0.1, 0.15, 0.20, 0.25 Jcm^{-2}. The laser pulses were repeated n = 1, 10, 20, 50, 100, 200 times with the frequency of 10 Hz, the pulse duration being 30 ns. Numerical calculations were applied to find the time and depth evolutions of temperature as described in [8]. For the fluences used and the repetition frequency of 10 Hz, the laser pulses are thermally independent. Therefore the total deposited energy is proportional to the number of pulses for a given fluence. In all samples, both Co (T_{melt} = 1768 K) and Ag (T_{melt} = 1235 K) layers melt at the fluence F=0.25 Jcm^{-2}. Co layers remain solid at F = 0.1, 0.15 and 0.2 Jcm^{-2} in all samples. Ag layers melt at F = 0.15 and 0.2 Jcm^{-2} both in Ag_2Co_1 and Ag_4Co_1 MLs while in Ag_6Co_1 ML, they do not melt at these fluences. Ag layers remain solid at F = 0.1 Jcm^{-2} in all samples. If Ag layers melt, they melt in the whole depth of MLs.

© Krystalografická společnost

The atomic structure of MLs was examined by XRD measured with CuK_α radiation both in the Bragg-Brentano (BB) and asymmetrical grazing incidence (GI) modes. The BB XRD was measured on a commercial powder diffractometer with a focusing graphite monochromator placed in the diffracted beam and a point NaI(Tl) scintillation detector. The GI XRD was measured on a laboratory-made diffractometer in the parallel beam geometry with a flat graphite monochromator in the primary beam. A very small divergence (~0.01°) was achieved by three fine parallel slits placed between the monochromator and the sample. A curved 120° position sensitive detector and a 12 kW rotating anode X-ray generator decreased the acquisition time considerably. The regularity of the ML stack and the quality of interfaces were investigated by specular XRR and GIDS measurements on a high-resolution diffractometer equipped with a double-crystal GaAs monochromator at $CuK_{\alpha 1}$ wavelength.

The electrical resistance *R(H)* was measured as a function of the applied magnetic field up to 50 kOe at 4.2 K using a standard four probe method with Ag contacts. Two geometries with magnetic field parallel or perpendicular to the sample surface were used. The GMR ratio was calculated as [*R(H)*-*R*(50 kOe)]/*R*(50 kOe). An example of the electrical resistance measurement in an external magnetic field is shown in Figure 1. The magnetization measurements were performed using a SQUID magnetometer between 4.2 and 300 K.

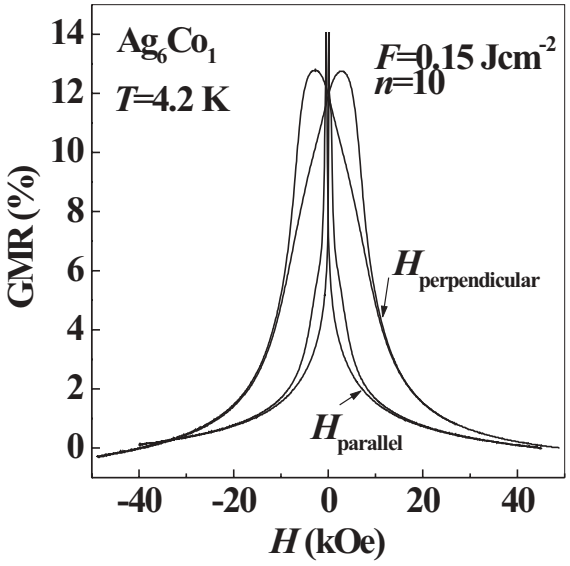

Figure 1. The electrical resistance of Ag_6Co_1 ML irradiated at $F = 0.15$ Jcm^{-2} and $n = 10$ pulses measured in parallel and perpendicular magnetic fields at 4.2 K.

3. Results

The GI XRD patterns for as-deposited Ag_2Co_1 and Ag_6Co_1 MLs taken at the angle of incidence $\alpha = 0.5°$ are shown in Figure 2. Both MLs exhibit a complete set of diffraction maxima of the face-centered cubic (fcc) Ag phase. Moreover, the maximum labelled as A may point at the presence of a small fraction of close-packed hexagonal (hcp) ordering (203 diffraction). This is not surprising as the fcc phase

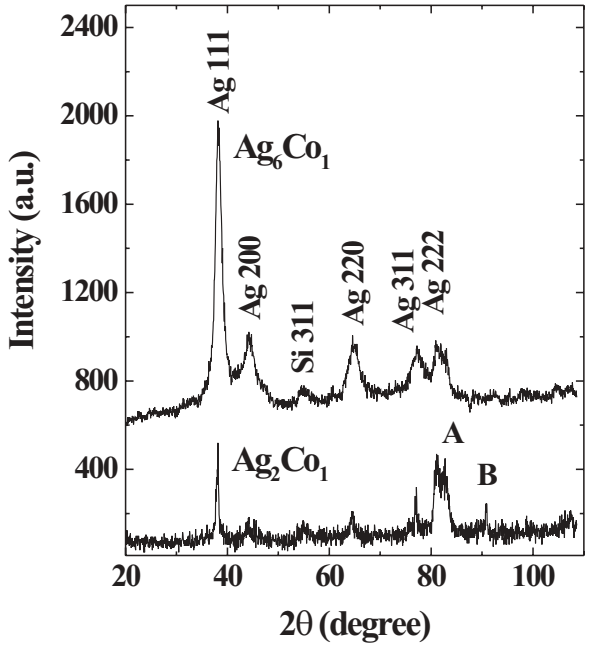

Figure 2. X-ray diffraction patterns taken at grazing angle of 0.5° for as-deposited Ag_2Co_1 and Ag_6Co_1 MLs. The curve for the latter is shifted upwards. 2θ is the angle between the primary and diffracted beams. The diffractions A and B are discussed in the text. Si 311 diffraction comes from the substrate.

in thin Ag layers is poorly developed and a tendency to another symmetry may easily be established. Co diffraction maxima are not seen due to the small thickness of Co layers and a low scattering power of Co atoms. Moreover, 200 diffraction of the fcc Ag phase partially overlaps with strong 002 hcp Co and 111 fcc Co diffractions. Thus only the maximum labelled as B may point at the presence of hcp ordering in Co layers in Ag_2Co_1 (200 diffraction). The polycrystalline structure of fcc Ag with random orientation of grains persists in Ag_2Co_1 and Ag_6Co_1 MLs also after the laser irradiation at $F = 0.2$ Jcm^{-2}. The presence of only distinct Ag diffractions after laser irradiation is in accordance with the immiscibility of Ag and Co following from the phase diagram.

A different structure of the layers was observed in Ag_4Co_1 ML. The BB XRD pattern of the as-deposited sample shows only 111 and 222 diffractions of fcc Ag (Figure 3). Moreover, the satellites around 111 diffraction are recognizable (see the inset in Figure 3). These features hint at a strongly textured (superlattice-like) structure with (111) planes in Ag grains oriented preferentially parallel to the surface. From the positions of the satellites of 111 diffraction, the ML period of ≈5 nm is calculated and from its integral width, the size of coherently scattering domains of 26 nm is estimated which covers ≈ 5 ML periods. For $F = 0.1$ Jcm^{-2}, the strongly textured structure is preserved up to $n =$ 200. For $F = 0.15$ Jcm^{-2}, it is gradually lost with increasing *n*. The satellites disappear and the 200 diffraction of fcc Ag emerges from the background. For $F = 0.2$ Jcm^{-2}, further Ag diffractions appear and the superlattice satellites are absent.

The specular XRR curves of as-deposited MLs as well as their evolution after $F = 0.15$ Jcm^{-2} irradiation are shown in Figure 4. For as-deposited Ag_4Co_1 ML (Figure 4b), the

© Krystalografická společnost

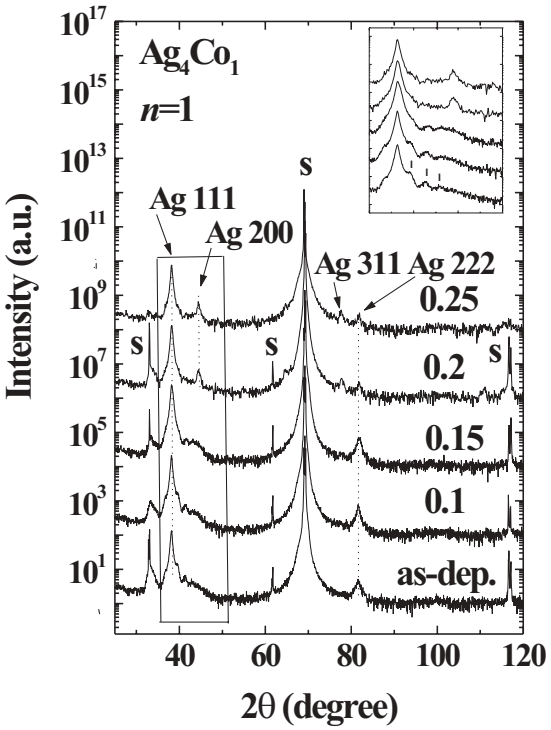

Figure 3. X-ray diffraction patterns taken in Bragg-Brentano geometry before and after one pulse irradiation with different fluences for Ag_4Co_1 ML. The curves for laser treated samples are shifted upwards. 2θ is the angle between the primary and diffracted beams. The superlattice satellites around Ag 111 diffraction are shown in more detail in the inset. The diffractions coming from the substrate are labelled as "s".

most distinct maximum comes from the ML period (the 1st Bragg maximum) while the smaller ones are connected with the total thickness of the ML stack (Kiessig maxima). The existence of two kinds of maxima points to a rather regular ML structure in the as-deposited Ag_4Co_1 ML. This is not observed in two other as-deposited MLs because of a smaller number of ML periods (Figures 4a and 4c). The XRR curves were simulated using the Fresnel optical computational code [9] to extract the basic ML parameters. The advantage of the optical approach is that it includes inherently refraction, extinction and absorption effects and is thus fully compatible with the dynamical theory of X-ray scattering. The interface roughness was included into the simulations by a Debye-Waller-like attenuation factor $\exp(-q_{j-1}q_j\sigma^2)$ [10] which modified the reflectivity coefficients of all interfaces, q_{j-1} and q_j being the scattering vectors above and below the *j*th interface, respectively, and σ being the root-mean-square roughness which was taken the same for all interfaces. This attenuation factor corresponds to the error function interface profile. The evolution of ML parameters with laser treatment is documented in Table 1. The period of as-deposited Ag_4Co_1 ML is consistent with the value assessed from the satellites around Ag 111 diffraction.

To characterize the interface morphology, non-specular scans at grazing incidence with a non-zero lateral (along the interfaces) component of the scattering vector are unavoidable. We traced the distribution of the scattered inten-

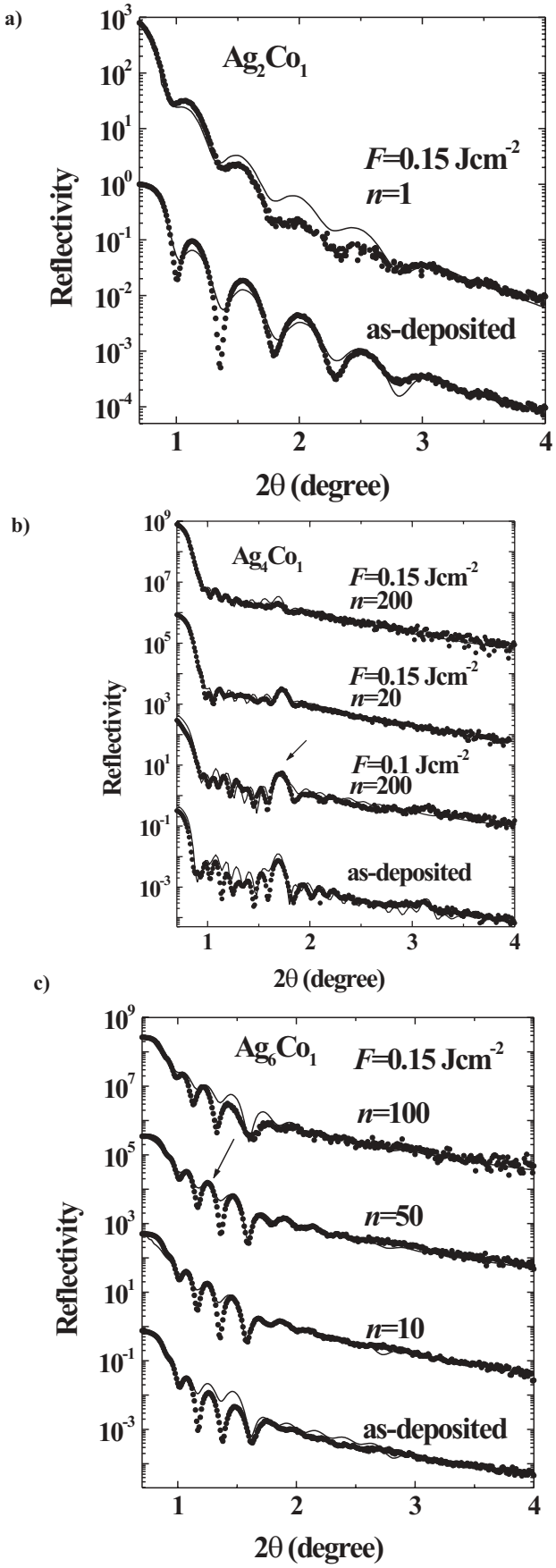

Figure 4. Evolution of specular XRR with laser irradiation for (a) Ag_2Co_1 (b) Ag_4Co_1, and (c) Ag_6Co_1 MLs. The measured curves (dots) were simulated by Fresnel optical computational code (line) and for laser treated samples they are shifted upwards. 2θ is the angle between the primary and diffracted beams. For the meaning of the arrows see Figure 5..

© Krystalografická společnost

Table 1

Evolution of ML parameters with laser irradiation obtained from the specular XRR simulations. *N, F, n, F_D, d, D,* σ stand for the number of periods, fluence, number of pulses, deposited energy, individual layer thickness, ML period, and interface roughness, respectively. The layer thicknesses were fixed randomly within 3-5 % interval around the starting values, indicated in the table, before entering the recursive procedure in the Fresnel optical computational code. An approximately linear decrease of the decrements of the refractive index across 5 (Ag_4Co_1) and 3 (Ag_2Co_1, Ag_6Co_1) upper layers towards the surface amounting to ≈ 30 % and ≈ 15 % at the surface, respectively, was included in the simulations. In Ag_4Co_1 exposed to $F = 0.1$ Jcm^{-2} and $n = 200$ irradiation, a linearly increasing thickness of the 5 upper layers reaching 4.9 nm (Ag) and 1.2 nm (Co) in the uppermost layers was also included. Due to a small amplitude of the XRR oscillations, the precision of the layer thickness determination in Ag_4Co_1 on the $F = 0.15$ Jcm^{-2} and $n = 200$ irradiation is rather low and reaches ±30%.

sample	*N*	*F* [Jcm^{-2}]	*n*	F_D [Jcm^{-2}]	d_{Ag} [nm]	d_{Co} [nm]	*D* [nm]	σ [nm]
Ag_2Co_1	5	0	0	0	2.1	1.2	3.3	1.0
		0.15	1	0.15	1.8	1.4	3.2	1.4
Ag_4Co_1	10	0	0	0	4.7	1.1	5.8	0.6
		0.1	200	20	4.65	1.0	5.65	0.6
		0.15	10	1.5	4.4	1.1	5.5	1.0
			20	3	4.4	1.1	5.5	1.1
			200	30	3.5	1.8	5.3	1.8
Ag_6Co_1	5	0	0	0	5.5	1.2	6.7	1.1
		0.15	10	1.5	5.2	1.6	6.8	1.2
			50	7.5	4.65	2.0	6.65	1.3
			100	15	4.0	2.5	6.5	1.3

Table 2

ML parameters obtained from the simulations of the X-ray diffuse scattering at grazing incidence. σ_r, ξ, L_{vert}, *and h* stand for the rms value of real (geometrical) interface roughness, lateral correlation length, vertical correlation length, and fractal parameter, respectively.

sample	*F* [Jcm^{-2}]	*n*	F_D [Jcm^{-2}]	σ_r[nm]	ξ [nm]	L_{vert} [nm]	*h*
Ag_4Co_1	0.1	0	0	0.6	60	58	1
		200	20	0.6	60	56.5	1
Ag_6Co_1	0.15	0	0	1.1	50	33	1
		50	7.5	1.3	10	1	1

sity throughout the reciprocal space by sample (detector) scans at a fixed detector (sample) position. Some examples of the sample scans for as-deposited and laser treated Ag_4Co_1 and Ag_6Co_1 MLs are shown in Figure 5. The central ridge is specular XRR broadened by the experimental resolution function and ML mosaicity. A curvature of the sample surface may eventually cause a deformation of this peak (splitting, asymmetry). The broad background (diffuse scattering) is due solely to the real (geometrical) interface roughness. Different frequency components of this roughness cause the wave vector transfer into different angles out of the specular direction. The diffuse scattering was simulated within the distorted-wave Born approximation (DWBA) to extract the parameters of the interface morphology and interface replication across the ML stack. The details of the calculations are described in [11]. We used the lateral (self) correlation function of the type

$$C(x) = \sigma_r^2 \exp -\left(\frac{x}{\xi}\right)^{2h} \quad (1)$$

for all interfaces where σ_r, x, ξ, h stand for the root-mean-square (rms) value of real interface roughness, lateral distance, lateral correlation length and fractal parameter, respectively, the last being related to the fractal dimension of an interface as $D = 3\text{-}h$. The vertical replication of the interface profiles was included in the simulations by a vertical (cross) correlation function [12]

$$C_j^k(x) = C(x) \exp -\left(\frac{|z_j - z_k|}{L_{vert}}\right) \quad (2)$$

© Krystalografická společnost

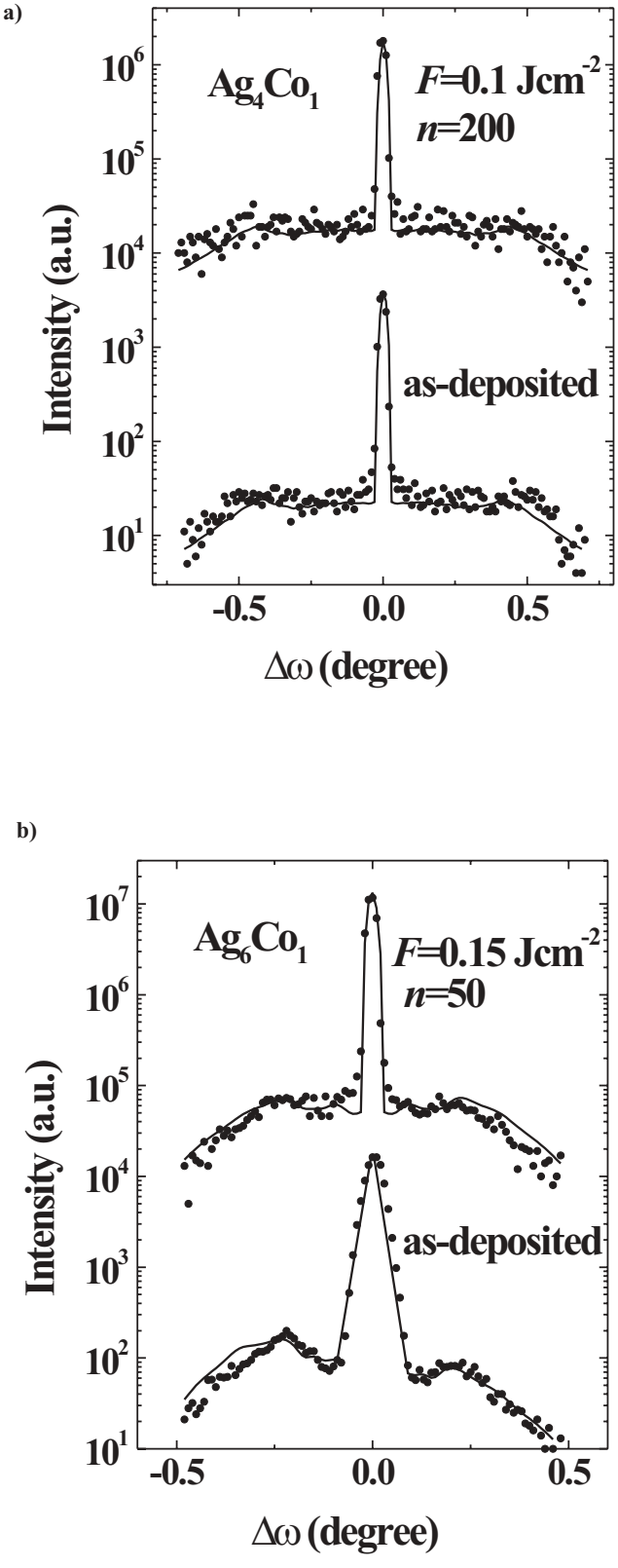

Figure 5. Sample scans for (a) Ag_4Co_1 and (b) Ag_6Co_1 MLs before and after a laser irradiation. The measured points (dots) were simulated within distorted-wave Born approximation (line) and for laser treated samples they are shifted upwards. Δω means the offset from the specular position. The detector was fixed at the positions shown in XRR curves (Figure 4) by the arrows.

where z_j is the vertical (perpendicular to the interfaces) coordinate of the mean jth interface and L_{vert} is the vertical correlation length (L_{vert}=0 ⇒ no replication of the interface profiles, $L_{vert}\rightarrow\infty$ ⇒ total replication). The parameters of some diffuse scattering simulations are given in Table 2. One can see that the interface morphology and its replication is changed considerably in laser treated Ag_6Co_1 ML only.

4. Discussion

From our previous GMR measurements [3,4] it follows that for Ag_2Co_1 ML, there is little possibility to change the GMR systematically with laser treatment. Ag layers start melting already for F = 0.15 Jcm^{-2} and no systematic change of the GMR occurs. For example, the original GMR of 11.5 % increases to 14.4 % for n = 1 and then decreases to 2.5 % for n = 100 at F = 0.15 Jcm^{-2}. For F = 0.2 Jcm^{-2}, the GMR reaches 7.6 % and 9.3 % for n = 5 and n = 20, respectively. The changes of the GMR ratio for Ag_4Co_1 ML are also not systematic but they are confined to a narrower interval around the original value even when the melting starts. For example, the original GMR of 5.8 % decreases to 4.7 % both for n = 1 and n = 20 at F = 0.15 Jcm^{-2}. For Ag_6Co_1 ML, the original GMR 7.6 % increases systematically with the supplied energy in the irradiation regime without melting, i.e. up to F = 0.2 Jcm^{-2}, being nearly doubled for n = 20 at this fluence (13.5 %). As the GMR effect originates from the spin-dependent interface electron scattering, its increase is determined by an increase of the interfacial area between non-magnetic and magnetic components. From this point of view, the breaking up of thin Co layers and formation of a discontinuous ML may explain the systematic GMR increase. In the following, we will inspect this point in more detail.

Laser treatment of Ag_6Co_1 ML before Ag layers start melting is connected with a decrease of Ag layer thicknesses while opposite is the case for Co layers, the ML period being generally reduced (Table 1). An enhanced decrement of the refractive index of Co layers in comparison with the theoretical one (by ≈10 %) had to be taken into account in the XRR simulations. These facts imply that Co layers are broken by Ag atoms penetrating between Co grains and a discontinuous multilayer is formed. Owing to the immiscibility of Ag and Co, grain boundary diffusion is the most probable mechanism. It can be seen that the thickness of such discontinuous Co layers is somewhat larger than in as-deposited state while Ag layers are gradually consumed. The ML character of the structure before Ag layers start melting is preserved.

The layer thicknesses may affect the GMR ratio in different ways. It is known that the GMR ratio exhibits an oscillatory behaviour with increasing Ag layer thickness the amplitude of which dies out above ≈ (4-5) nm [13]. Contrarily, the GMR ratio always decreases with increasing thickness of the magnetic layer. One can see from Table 1 that no significant change of the GMR due to the change of the Ag layer thicknesses in the given interval (4-5.5) nm can be expected. On the other hand, an increase of the Co layer thicknesses with increasing number of pulses

© Krystalografická společnost

(1.2-2.5) nm would imply a strong decrease of the GMR. This is just opposite to what we have found [3, 4] which also indicates the formation of a discontinuous multilayer. Moreover, the quantity of the GMR increase, which amounts to nearly 100%., cannot be explained in no other way than by the formation of a discontinuous multilayer as it has been shown already by Hylton at al. [14].

Ag_2Co_1 ML has a similar atomic structure of Ag layers as Ag_6Co_1 but there is a substantially smaller interval of laser fluences where the diffusion process in solid state is possible. Ag_2Co_1 ML is heavily disturbed already after F = 0.15 Jcm^{-2} and n = 1 irradiation when the melting of rather thin Ag layers starts. The increase of the Co layer thicknesses at the expense of the Ag ones and increased interface roughness hint at the mixing of liquid Ag/solid Co interfaces which prevents from the formation of a discontinuous ML. A highly non-equilibrium process of melting and rapid solidification on each laser pulse results into a recrystallized structure composed of Ag and Co granules (clusters) the parameters of which cannot be controlled in a predictable way. These parameters like number, sizes, shapes and distribution of Co clusters determine the GMR value. Consequently, the GMR evolution on laser treatment is not systematic for Ag_2Co_1 ML.

The reduction of the Ag layer thicknesses in Ag_4Co_1 ML for F = 0.1 Jcm^{-2} irradiation is not accompanied by an increase of the Co layer thicknesses and may be ascribed to the annealing-out of defects in Ag layers. The satellites around 111 diffraction of fcc Ag persist up to F = 0.15 Jcm^{-2} and n = 20 irradiation. Therefore, not only ML structure evidenced by the XRR but also its superlattice-like character is preserved. The strong texture obviously stabilizes the original structure even when melting starts. Only for F = 0.15 Jcm^{-2} and n = 200 irradiation, the texture is suppressed and the formation of a granular-like structure starts, similarly as in Ag_2Co_1 ML. Up to this point, the GMR of Ag_4Co_1 ML changes non-systematically but much less than for Ag_2Co_1 ML.

The XRR simulations were improved, especially at low scattering angles, when an approximately linear decrease of the decrements of the refractive index across 5 (Ag_4Co_1) and 3 (Ag_2Co_1, Ag_6Co_1) upper layers was included, the total decrease in the uppermost layer being ≈30 % and ≈15 %, respectively. This result indicates surface oxidation due to the ageing of the samples which can be expected in Ag/Co multilayers. In Ag_4Co_1 exposed to F = 0.1 Jcm^{-2} and n = 200 irradiation, a linearly increasing thickness of the 5 upper layers reaching 4.9 nm (Ag) and 1.2 nm (Co) in the uppermost layers was also included.

Owing to the immiscibility of Ag and Co, the interface morphology is fully controlled by the crystalline grains inside the layers. This conclusion is supported by the fact that the interface roughness σ determined from the XRR simulations is equal to the real (geometrical) one σ_r obtained from the GIDS simulations for all samples. Thus any change of the interface correlation is closely related to the grain morphology and size evolution induced by laser treatment. For Ag_6Co_1 ML, the vertical correlation length, comparable with the total ML thickness in as-deposited state, deceases to the level of Co layer thickness for F = 0.15 Jcm^{-2} and n = 50 irradiation (Table 2). This means that grain boundary diffusion breaks the replication of interface profiles completely. Simultaneously, the lateral correlation length decreases 5 times which indicates the formation of smaller grains in discontinuous ML that promotes the GMR ratio. A small value of interface roughness in as-deposited Ag_4Co_1 ML is due to the brick-like shaped and nearly parallelly ordered Ag grains observed by cross sectional transmission electron microscopy [4]. The value of such small interface roughness is probably controlled by perfection of the grain connections rather than by the grains themselves. Contrary to Ag_6Co_1 ML, the vertical and lateral correlation lengths of interface profiles are little affected by laser treatment.

For all samples, fractal parameter h = 1 so that fractal and topological interface dimensions are the same. This finding means that the interface profiles vary rather smoothly in lateral direction in the sense that no jaggedness typical for fractal behaviour occurs.

5. Conclusions

The behaviour of the GMR in Ag/Co MLs after excimer laser irradiation is closely related to the structural evolution which is determined by the atomic structure and thicknesses of the layers in as-deposited state. In Ag_6Co_1 ML with random polycrystalline structure, the GMR ratio increases systematically before Ag layers start melting. We have shown that the formation of a discontinuous ML, which takes place via grain boundary diffusion, is responsible for the GMR increase. Such a structure is in a way similar to that in granular thin films exhibiting the GMR effect. The formation of a discontinuous ML cannot be completed in Ag_2Co_1 ML where the melting starts at a low laser fluence. In Ag_4Co_1 ML, as-deposited structure is strongly textured which prevents from grain boundary diffusion of Ag into Co and stabilizes the ML structure. Thus a controlled optimization of the GMR ratio is possible neither in Ag_2Co_1 nor Ag_4Co_1 MLs, though because of different reasons.

As soon as Ag layers start melting, the ML structure is lost and a granular-like structure is established. The parameters of this recrystallized structure, resulting from a highly non-equilibrium process, are rather random and have no direct link with the structure observed before the melting starts. Thus a controlled optimization of the GMR is difficult.

Acknowledgements

The authors acknowledge a partial support from the Slovak scientific grant agency VEGA (project no. 5083/98), the Grant agency of the Czech Republic (project no. 101/98/0553) and NATO linkage grant no. HTECH.LG 971726.

© Krystalografická společnost

References

1. M.N. Baibich, J. Brotto, A. Fert, F. Nguyen van Dau, F. Petroff, P. Etienne, G. Creuzet, A. Friedrich, J. Chazelas, *Phys. Rev. Lett.*, **61** (1988) 2472-2474.
2. R.E. Camley, J. Barnas, *Phys. Rev. Lett.*, **63** (1989) 664-6463.
3. Š. Luby, E. Majková, M. Spasova, M. Jergel, R. Senderák, E. D'Anna, A.Luches, M. Martino, M. Brunel, I.M.Dmitrenko, *Thin Sol. Films*, **312** (1998) 15-19.
4. E. Majková, M. Spasova, M. Jergel, Š. Luby, S. Okayasu, A.Luches, M. Martino, E.N. Zubarev, M. Brunel, *Thin Sol. Films*, **343&344** (1999) pp. 211-214.
5. J.D. Jarrat, J.A. Barnard, *J. Appl. Phys.*, **79** (1996) 5606-569.
6. M. Iijima, Y. Shimizu, N. Kojima, A. Tanaka, K. Kobayashi, *J. Appl. Phys.*, **79** (1996) 5602-5605.
7. Shi-Ming Zhou, Yu Wang,, Wei-Rong Zhu, Rong-Jun Zhang, Yu-Xiang Zheng, Quing-Yuan Jin, Liang-Yao Chen, Biao You, Wu Ji, An Hu, Hongru Zhai, Honghi Shen, *J. Appl. Phys.*, **83** (1998) 900-905.
8. E. D'Anna, S. Luby, A. Luches, E. Majkova, M. Martino, *Appl. Physic*s, A **56** (1993) 429-435.
9. J.H. Underwood, T.W. Barbee Jr., *AIP Conf. Proc.*, **75** (1981) 170-178.
10. L.Névot, P.Croce, *Rev.Phys.Appl.,* **15** (1980) 761-779.
11. M. Jergel, V. Holý, E. Majková, Š. Luby, R.Senderák, H.J.Stock, D.Menke, U.Kleineberg, U.Heinzmann, *Physica*, B **253** (1998) 28-39.
12. Z.H. Ming, A. Krol, Y.L. Soo, H. Kao, J.S. Park, K.L. Wang, *Phys. Rev.*, B **47** (1993) 16373-16381.
13. A. Fert, A. Barthelemy, P. Etienne, S. Lequien, R. Loloee, D.K. Lottis, D.H. Mosca, F. Petroff, W.P. Pratt, P.A. Schroeder, *J. Magn.&Magn. Mat.,* **104-107** (1992) 1712-1715.
14. T.R. Hylton, K.R. Coffey, M.A.Parker, J.K. Howard, *J. Appl. Phys.,* **75** (1994) 7058-7063.

© Krystalografická společnost